Applied Catalysis A, General 592 (2020) 117369

Contents lists available at ScienceDirect

Applied Catalysis A, General

journal homepage: www.elsevier.com/locate/apcata

Hydrophobic functionalization of HY zeolites for efficient conversion of glycerol to solketal

Mohammad Shahinur Rahaman[a], Thanh Khoa Phung[a,b,c], Md. Anwar Hossain[a], Emtias Chowdhury[d], Sarttrawut Tulaphol[a,e], Shashi B. Lalvani[f], Martin O'Toole[d], Gerald A. Willing[a], Jacek B. Jasinski[b], Mark Crocker[g,h], Noppadon Sathitsuksanoh[a,*]

[a] Department of Chemical Engineering, University of Louisville, Louisville, KY, 40292, USA
[b] Conn Center for Renewable Energy Research, University of Louisville, Louisville, KY, 40292, USA
[c] School of Biotechnology, International University, Vietnam National University, HCMC, Quarter 6, Linh Trung Ward, Thu Duc District, Ho Chi Minh City, Vietnam
[d] Department of Bioengineering, University of Louisville, Louisville, KY, 40292, USA
[e] Department of Chemistry, King Mongkut's University of Technology Thonburi, Bangkok, 10140, Thailand
[f] Department of Chemical, Paper, and Biomedical Engineering, Miami University, Oxford, OH, 45056, USA
[g] Center for Applied Energy Research, University of Kentucky, 2540 Research Park Drive, Lexington, KY, 40511, USA
[h] Department of Chemistry, University of Kentucky, Lexington, KY, 40506, USA

ARTICLE INFO

Keywords:
Solketal
Hydrophobic
HY zeolites
Emulsion
Glycerol acetalization
Mass transfer

ABSTRACT

Production of solketal by glycerol acetalization is a promising pathway to add values to glycerol. Our evidence indicated that, initially, the reaction was limited by poor interfacial mass transfer. Acetone slowly diffused and solubilized in the glycerol phase, where it reached the catalyst's active sites to form solketal. We describe a strategy that overcomes this interfacial mass transfer limitation by grafting an organosilane surfactant (n-octadecyltrichlorosilane (OTS)) onto the surface of an HY catalyst. The OTS-grafted HY catalyst became hydrophobic and assisted in emulsion formation between the two immiscible reactants, minimizing the interfacial mass transfer limitation. As a result, the OTS-HY catalyst produced high catalytic activity (89% conversion) compared with that of HY (28% conversion) at 30 °C after 60 min. The high catalytic activity of organosilane-modified HY catalyst at low temperature makes it a promising candidate for other acid-catalysed two-phase reactions.

1. Introduction

The petroleum and animal farming industries are the leading contributors to greenhouse gases, including carbon dioxide (CO_2), methane, and nitrous oxide [1,2]. Carbon dioxide emissions account for 65% of global greenhouse gases, causing a global temperature rise and climate change and negatively affecting agricultural/forest production, livestock farming, and our standard of living [3–5]. In 2014, CO_2 emissions were estimated at ~34.1 gigatonnes [6], and this quantity is projected to rise [7]. CO_2 emissions stem from fossil fuel processing and methane release from shale oil extraction and natural gas development [8]. Production of biofuels and bioproducts from renewable plant biomass can reduce CO_2 emissions, mitigating global warming and climate change.

Glycerol is a by-product of processing vegetable oils to produce biodiesel. In 2017, the biodiesel production volume was ~ 1.6 billion gallons, and production is projected to reach 4 billion gallons by 2022 [9]. Biodiesel production generates ~10 wt.% glycerol [10]. As our society slowly moves to a sustainable future, the ability to convert glycerol to high-value products will accelerate its commercial use and the fight against global warming.

Glycerol can be upgraded to valuable compounds such as propanediol, acrolein, glycerol carbonate, glyceric acid, tartronic acid, syngas, and solketal [11–19], thereby providing opportunities for additional revenue for the biodiesel industry and the agricultural sector. Glycerol acetalization is catalyzed by acid sites and produces cyclic acetals with 5- and 6-membered rings (4-hydroxymethyl-2,2-dimethyl-1,3-dioxane (solketal) and 5-hydroxy-2,2-dimethyl-1,3-dioxane (acetal)) (Fig. 1). Solketal is of particular interest because (1) it is a 100% bio-based chemical, produced from glycerol conversion with acetone. Acetone can be derived from hemicellulose from biorefineries [20]; (2) the reaction operates under mild conditions [21–23]; and (3)

* Corresponding author.
E-mail address: n.sathitsuksanoh@louisville.edu (N. Sathitsuksanoh).

https://doi.org/10.1016/j.apcata.2019.117369
Received 30 August 2019; Received in revised form 21 November 2019; Accepted 29 November 2019
Available online 07 January 2020
0926-860X/

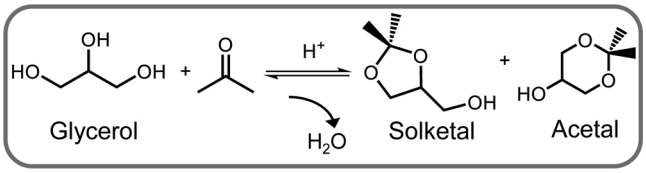

Fig. 1. Solketal production from glycerol acetalization by acid.

solketal can be used in many applications including fuel additives [24,25], solvents in paint and ink industries [26–28], cleaning products [29], additives for the pharmaceutical industry [30,31], and co-initiators for polymerization [29,32].

Although homogeneous acid catalytic systems work for glycerol acetalization, their use is complicated by the need to separate catalysts from products. Thus, heterogeneous zeolite catalysts have been popular choices for glycerol acetalization [33,34]. However, the low glycerol solubility in acetone (5 wt.% or ~ 0.03 glycerol/acetone molar ratio) causes the two reactants to be immiscible, presenting a mass transfer limitation. Immiscibility greatly limits the joint contact between the two reactants and catalysts' active sites, and, therefore, impairs catalysis [35–37]. Mass transfer limitation is unavoidable in multiphase reactions, including glycerol acetalization, but it can be minimized [38,39].

The objective of this study was to develop a multifunctional, solid acid catalyst modified with a surfactant to improve the contact between glycerol and acetone. We hypothesized that grafting an organosilane surfactant onto a solid HY zeolite catalyst would generate interface-active materials that would create an emulsion in which catalysis would occur. The emulsion would enhance the interfacial mass transfer by increasing the contact surface between the two immiscible reactants.

We tested the foregoing conjecture by grafting an organosilane surfactant, n-octadecyltrichlorosilane (OTS), onto an HY zeolite catalyst and evaluated the performance of this OTS-grafted HY (OTS-HY) at 30 °C. We selected OTS because it has a long alkyl chain to provide substantial hydrophobicity. Moreover, we selected HY zeolite (Si/Al = 2.6) as our catalyst because (1) it is widely used in the chemical industry, (2) it has a large pore dimension (7.3 nm), and (3) it has a low Si/Al ratio, providing a high acidity (578 μmol NH_3/g catalyst) [40] for glycerol acetalization. We found that the OTS-HY catalyst produced a higher glycerol conversion than did the HY catalyst. The OTS-HY catalyst enabled emulsion formation, increasing contact between the two reactants. This catalytic system addresses the fundamental limitation of the low contact between a catalyst's active sites and the two immiscible reactants in glycerol acetalization.

2. Materials and methods

2.1. Functionalization of zeolites with surfactant

HY zeolite (CBV600, Si/Al ratio = 2.6) was obtained from Zeolyst® International (Conshohocken, PA, USA). We chose this HY zeolite with 2.6 Si/Al ratio because it has a high acid site density with the hydrophilic characteristic, enabling us to observe (1) the negative effect of water formation on catalytic activity and (2) the benefit of adding surface hydrophobicity. The as-received HY zeolite was calcined at 500 °C for 1 h to remove residual impurities before use. The surface functionalization of the zeolite was performed as described [41]. In short, 1 g of zeolite was dispersed in 20 mL of toluene in a capped 250 mL flask using a sonicator at room temperature for 1 h. The organosilane reagent (n-octadecyltrichlorosilane (OTS), 95%, Alfa Aesar) at an organosilane/zeolite ratio of 0.5 mmol/g zeolite (theoretical OTS loading on zeolite) was mixed with 50 mL toluene at room temperature. The hydrolyzable Cl ions of the OTS underwent hydrolysis and formed a stable condensation with silanol groups (-Si-OH) on the surface of HY. The organofunctional group (octadecyl) is a nonhydrolyzable organic radical and adds chemical characteristics. The organosilane solution was added to the zeolite suspension, and the resulting mixture was stirred for 24 h at 500 rpm at room temperature. The surface-modified zeolite was then filtered and washed with ethanol five times and vacuum dried at 80 °C overnight. This functionalized zeolite was named OTS-HY.

2.2. Characterization of catalytic materials

The degree of hydrophobicity of zeolites was determined by the contact angle measurement using water droplets. Zeolite samples were compressed into a 1 cm disc (OD) with a thickness of 2 mm. A 1 μL water droplet was placed on the external surface of the disc using Optical contact angle measurement and drop contour analysis (OCA15, DataPhysics Instruments USA Corp., Charlotte, NC, USA). Infrared spectra of the zeolites were recorded on a JASCO Fourier transform infrared (FTIR) spectrometer (Easton, MD, USA), equipped with an attenuated total reflection stage (ATR). High-resolution transmission electron microscopy (HRTEM) was performed on catalysts using a 200 kV-operated field emission gun FEI Tecanai F20 transmission electron microscope. Low-intensity illumination conditions were used to minimize the amorphization of zeolites.

To confirm the changes in surface functionality after grafting OTS onto HY catalysts, the diffuse reflectance infrared Fourier transformation spectroscopy (DRIFT) was performed using the JASCO FTIR equipped with high-temperature DiffuseIR™ cell (PIKE Technology, WI, USA). The sample treatment and temperature program were described elsewhere with a slight modification [41]. In short, all experiments were performed after heating 5 mg catalyst sample in situ up to 230 °C under a flow of N_2 (20 mL/min) with a heating rate of 10 °C/min. Then the temperature was maintained at 230 °C for 30 min. A background spectrum was recorded prior to each run and the 512 scans of spectra were collected in the range between $4000-1000\,cm^{-1}$ at a $4\,cm^{-1}$ resolution.

The surface area and pore volume of zeolites were measured using N_2 adsorption/desorption by a Tristar Micromeritics (Norcross, GA, USA) instrument. Prior to the measurement, the samples were pretreated at 160 °C for 2 h using a Micromeritics FlowPrep with sample degasser (Norcross, GA, USA). The surface area, S_{BET}, was determined by N_2 isotherms using the Brunauer–Emmett–Teller equation (BET) on the basis of overall mass of the catalysts. The desorption cumulative pore volume was estimated according to the Barrett–Joyner–Halenda (BJH) model. The moisture and organic compounds on the catalysts were determined by thermogravimetric analysis (TGA) using a SDT Q600 TA instrument (New Castle, DE, USA). In short, ~20 mg of the sample was placed in a cylindrical alumina crucible and heated in the air from room temperature to 500 °C with a heating rate of 10 °C/min under N_2 flow (100 ml/min). The moisture content of catalyst was calculated from the weight loss below 150 °C. X-ray diffraction (XRD) analysis was performed on a Bruker D8 Discover diffractometer (Bellerica, MA, USA) using CuKα radiation and 2θ ranging from 10° to 60° with 0.2 s/step [41]. This 2θ range revealed the diffraction intensity of (220), (311), (331), (511), (440), (533), (642), and (555), respectively [42–44]. The suspension behavior of OTS-HY and HY catalysts was investigated by placing catalysts in the glycerol-acetone system (1/1 v/v). Videos 1 and 2 show the catalyst behavior in both phases (see *Supplementary information*).

The total acidity of zeolites was determined by ammonia-temperature programmed desorption (NH_3-TPD). The NH_3-TPD experiments were performed using a Micromeritics ChemiSorb 2720 instrument equipped with a thermal conductivity detector (TCD) (Norcross, GA, USA). The samples were dried in a vacuum oven overnight prior to NH_3-TPD. About 20 – 40 mg of sample was pretreated at 250 °C for 1 h under flowing He gas to remove adsorbed water. The sample was then cooled to 100 °C and saturated with ammonia (10% NH_3/He). Next, the samples were flushed with 40 mL/min He flow at 100 °C for 1 h to

remove physically adsorbed ammonia. TPD profiles were recorded by heating the samples to 700 °C at a rate of 10 °C/min in 40 mL/min He flow. In the case of OTS-HY catalysts, we ran the TPD experiment without pre-adsorption of NH_3 to evaluate the OTS decomposition temperature ranges and its contribution during the NH_3-TPD. To determine the acid site density of OTS-HY catalyst, we subtracted the OTS decomposition peak area from the NH_3-TPD peak area.

2.3. Study of glycerol acetalization

Reactions were performed in 15 mL glass pressure vials in an oil bath. Typically, glycerol, acetone, and catalysts were added to the pressure vial which was sealed and stirred at the desired temperature. We ran this reaction for different times (10 − 60 min), at different temperatures (30 and 50 °C), with different catalyst loading (5 and 15 wt.%), and a fixed glycerol/acetone molar ratio of 1/12 (12 wt.% glycerol), unless otherwise noted. The OTS-HY catalyst was loaded at an amount that provided a number of active sites comparable to that of HY. Dodecane was used as an internal standard. The glycerol conversion and product yield were calculated based on the internal standard. The reaction was stopped by quenching in a cold-water bath followed by adding ethanol (2 mL ethanol per 0.25 g glycerol) to dissolve the remaining glycerol and acetone. The solution was centrifuged, and the solid catalyst was removed. The liquid sample was then diluted with ethanol prior to analysis.

The reactants and products were analyzed using a gas chromatograph (7890B GC) (Agilent Technologies, Santa Clara, CA, USA) equipped with a mass spectrometer and flame ionization detector (FID) for product identification and quantification, respectively. A DB-1701 column (30 m x0.25 mm x0.25 µm, Agilent Technologies, Santa Clara, CA, USA) was used for product separation with the following parameters: injection temperature 275 °C and FID detector temperature 300 °C; split ratio 1:50. The temperature program started at 50 °C with a heating rate of 8 °C/min to 200 °C. The glycerol conversion, product yield, and product selectivity were calculated as follows:

$$\text{Glycerol conversion (\%)} = \frac{\text{mole of glycerol reacted}}{\text{initial mole of glycerol}} \text{x100}$$

$$\text{Product yield (\%)} = \frac{\text{mole of product generated}}{\text{initial mole of glycerol}} \text{x100}$$

$$\text{Product selectivity (\%)} = \frac{\text{Product yield}}{\text{Glycerol conversion}} \text{x100}$$

3. Results and discussion

We first confirmed the successful grafting of the OTS surfactant onto the HY catalyst and characterized changes in the surface properties. These analyses were performed with Fourier-transform infrared spectroscopy (FTIR), Thermal gravimetric analysis (TGA), High-resolution transmission electron microscope (HRTEM), X-ray diffraction (XRD), and N_2-adsorption/desorption. Then we evaluated the effect of OTS grafting onto the HY catalyst in the glycerol acetalization reaction with various conditions.

3.1. Characterization of the organosilane–grafted HY zeolites

The FTIR and DRIFT spectra of the OTS-HY catalyst confirmed the successful grafting of OTS onto the HY catalyst. The skeletal FTIR spectra of the unmodified HY catalyst presented an asymmetric stretching of the T−O−T bridges at 1056 and 1198 cm^{-1} (Fig. 2B), where T is tetrahedrally coordinated Si or Al atoms [45,46]. Upon OTS grafting onto HY catalyst, the characteristic T−O−T band at 1056 cm^{-1} shifted to 1050 cm^{-1} because of the formation of the Si-O bond on the tetrahedral T−O−T. We observed a similar down-shift of the zeolite's characteristic T−O−T band in the silane grafted SAPO-34 zeolites, suggesting the formation of linkages between silane and zeolites [47]. We observed bands at 2919 and 2851 cm^{-1}, associated with the CH symmetric (υ_s(CH)) and asymmetric (υ_a(CH)) stretching vibrations for CH_2 groups of the OTS, respectively (Fig. S1A). The band at 1198 cm^{-1} was due to the formation of Si-O-Si linkages between OTS and HY catalyst [48,49]. We did not observe the characteristic band of the self-condensed OTS product at 1014 cm^{-1}, suggesting that its formation was negligible (*see Supplementary information*, Fig. S1B).

We further confirmed the successful OTS grafting by DRIFT and observed changes in the OH vibrational region (3500–3800 cm^{-1}) of HY and OTS-HY catalysts. We detected a significant decrease in band intensity at 3740 cm^{-1} after OTS grafting onto HY catalysts (Fig. 2C). Whereas the two bands at 3627 and 3562 cm^{-1} remained relatively unchanged. The band at 3740 cm^{-1} was attributed to the free silanol groups on the external surface of HY catalysts [50]. So the decrease in this band intensity indicated a reduction in density of silanol groups after OTS grafting. The bands at 3627 and 3562 cm^{-1} were attributed to the structural hydroxyl groups, the high-frequency (HF) OH groups at the supercages and low frequency (LF) at the sodalite cages, respectively [51]. These OH groups are responsible for the Brønsted acidity of the zeolites [52,53]. After OTS grafting, intensities of these bands remained relatively unchanged, suggesting that grafted OTS did not block the active sites. Consistent with our results, Zapata et al. also observed negligible changes in intensities of these OH stretching bands after silylation of HY catalysts [41]. The retention of the active sites in OTS-HY catalysts was helpful for the acetalization reaction. Hence, alterations of FTIR bands in the fingerprint region and the reduction of the silanol density observed by DRIFT confirmed the formation of linkages between OTS and HY catalysts.

We used TGA to assess the stability of the OTS-HY and quantify the amount of OTS grafted onto the HY (Fig. 2A). Below 150 °C, HY incurred an initial weight loss (~5%) that was attributed to breaking hydrogen-bond networks and desorption of water. OTS-HY's weight loss was lower (~2%). The sharper decrease in weight of HY indicated higher water adsorption (~5%) compared with that of OTS-HY (~2%). These results suggested that OTS-HY catalyst was more hydrophobic than HY catalyst because the surface of HY catalyst consists of portions of free silanols (-Si-OH) that adsorb water molecules [54–56]. The weight loss of the OTS-HY occurred in three steps: (1) ambient to 150 °C, (2) 150 − 270 °C and (3) 400 − 500 °C. The weight losses in the first and second steps were from the evaporation of moisture and residue organic solvent during synthesis, respectively. The total weight loss for OTS-HY was higher than that of HY, which we attributed to the slow decomposition of OTS at a higher temperature (> 400 °C). Zapata et al. reported OTS decomposition from OTS-functionalized HY in the range of 350–600 °C [59], corroborating our OTS decomposition findings. We estimated that the amount of grafted OTS on HY was ~16% (w/w).

The crystallinity of HY was preserved after grafting with OTS. The HRTEM image (Fig. 3A & D) of OTS-HY catalyst illustrated (1) the cubic crystalline structure of the FAU zeolites [43,57], and (2) an unchanged crystalline structure after grafting OTS. Likewise, the XRD spectrum of OTS-HY catalyst confirmed the presence of a highly crystalline HY zeolite [58] (Fig. 4). The HRTEM and XRD results suggested a negligible loss of crystallinity after grafting OTS onto HY.

To evaluate how grafting OTS onto HY affected the catalyst's acid sites, we measured changes in surface area, pore-volume, and acidity by N_2-adsorption/desorption and NH_3-TPD. The N_2 adsorption/desorption isotherms of HY and OTS-HY catalysts exhibited the type IV isotherm [43], indicating that both catalysts were microporous (Fig. S2). The estimated surface area and pore volume of HY zeolite were 513 m^2/g and 0.36 cm^3/g (Table 1), consistent with reported values [40]. Previous investigators reported that grafting organosilanes onto zeolites reduced the surface area and pore volume because some portion of the pores was occupied by the organosilanes [41]. In addition, we

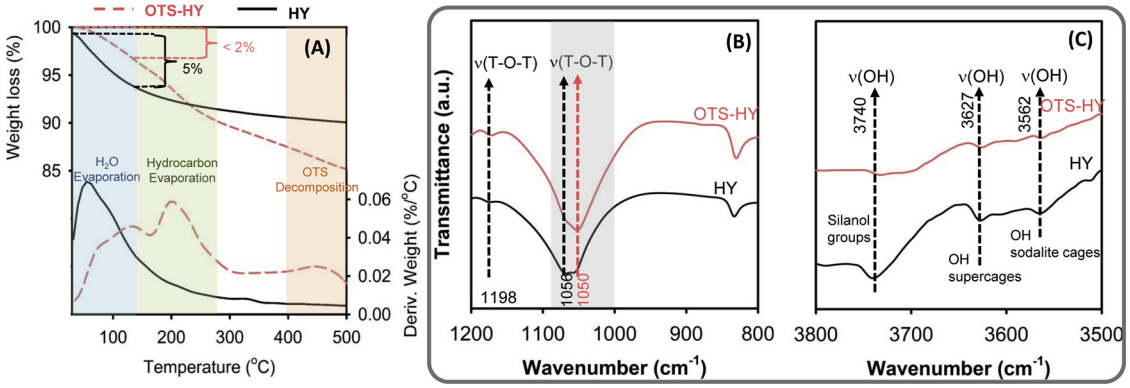

Fig. 2. TGA profiles (A), FTIR spectra (B), and DRIFT spectra (C) of OTS-HY and HY catalysts.

speculated that the decrease in the surface area and pore volume of our OTS-HY catalysts might be partly because of the dilution contributed from the grafted OTS. Moreover, our results revealed a slight decrease in the total acidity of OTS-HY catalysts (552 μmol NH_3/g catalyst), measured by NH_3-TPD, compared with that of HY catalyst (578 μmol NH_3/g catalyst), and this behavior is consistent with previous observations [41,59]. The slight change in the total acidity of the OTS-HY catalysts agreed with our DRIFT results, showing comparable skeleton OH groups (i.e., at 3627 and 3562 cm^{-1}) and suggesting the retention of acidity after the OTS grafting. We found that the grafting OTS onto HY took place mostly on the external surface of the HY catalysts, leaving the Brønsted and Lewis acid sites intact.

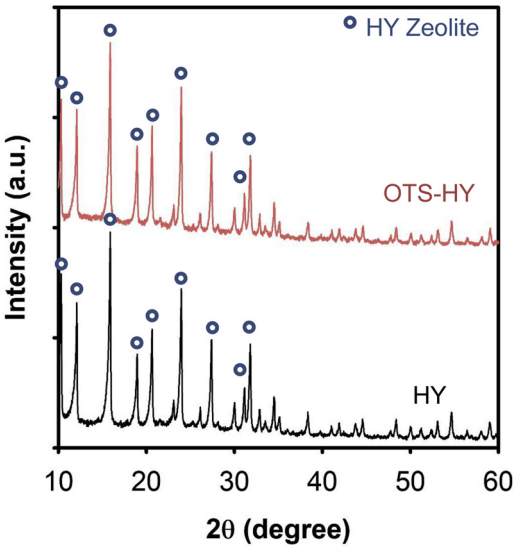

Fig. 4. XRD patterns of OTS-HY and HY catalysts.

3.2. Emulsion formation by modified catalysts in two-phase systems

Typically, the HY catalyst contains many free silanols, making it hydrophilic and limiting its suspension in the less polar acetone phase. Thus, we investigated the catalyst suspension behaviour by placing HY and OTS-HY in two liquid systems, (1) water-dodecane, and (2) glycerol-acetone. We chose the water-dodecane system to represent the polar-nonpolar solvent system. In the water-dodecane system, the OTS-HY catalyst was suspended in dodecane, whereas the HY was suspended in water (Fig. S3A & B). These visual observations were consistent with

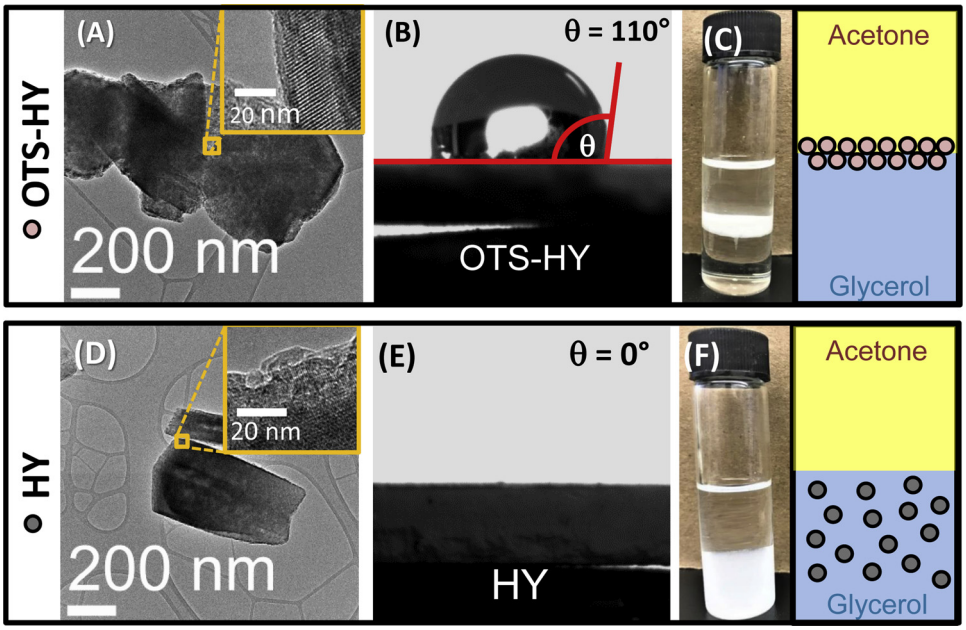

Fig. 3. HRTEM images of HY and OTS-HY catalysts (A & D) and their contact angles (B & E). The suspension behaviour of HY and OTS-HY catalysts in the glycerol-acetone system (C & F).

Table 1
Surface properties and acidity of HY and OTS-HY catalysts.

Catalyst	S_{BET} (m^2/g)	V_{pore} (cm^3/g)	V_{micro} (cm^3/g)	d_{pore} (Å)	Acidity (μmol NH_3/g catalyst)		
					Weak	Strong	Total
HY	513	0.36	0.22	7.3	265	313	578
OTS-HY	347	0.23	0.14	6.5	286	267	552

Note: S_{BET} = surface area; V_{pore} = pore volume; V_{micro} = micropore volume; d_{pore} = pore diameter.

the expectation that grafting OTS onto HY would add a hydrophobic layer to the HY surface, enabling it to be suspended in the nonpolar dodecane phase. These results agreed Zapata et al. who showed that. in a water-decalin system, a pristine hydrophilic catalyst settled in the water phase [59], whereas an organosilane-grafted catalyst dispersed in the decalin phase.

To determine the degree of hydrophobicity of our OTS-HY catalyst, we measured its contact angle and observed its behaviour in the two-phase systems. The OTS-HY had a contact angle of ~110°, suggesting that OTS-HY was hydrophobic [60] (Fig. 3B). The water droplet for HY adsorbed into the disc, i.e., the contact angle was ~0° (Fig. 3E). Our contact angle results agreed with another study by Zapata et al. [41] that showed a high degree of hydrophobicity of OTS-grafted HY catalyst (126-135°). In addition, we conducted the water adsorption experiments using the OTS-HY and HY catalysts in a closed container with 100 mL DI water in a 200 mL beaker and measured the water absorption during 12 h. The pristine HY catalyst had ~3 times higher water adsorption capacity than the OTS-HY catalyst (Fig. S4), an observation that corresponded with the TGA results. These results confirmed the high degree of hydrophobicity of OTS-HY and the hydrophilicity of HY. Nonetheless, these water adsorption results suggested that OTS-HY was not completely hydrophobic because water could still adsorb onto its surface.

The locations of the OTS-HY and HY catalysts in the reaction vessel further confirmed the difference in the catalysts' surface properties. The glycerol-acetone system was a two-phase system due to low glycerol solubility in acetone. The OTS-HY catalyst was suspended at the interface between glycerol and acetone (Fig. 3C) because, although acetone is a polar solvent, it is less polar than glycerol. Hence, OTS-HY did not disperse in the acetone (Fig. 3F). Conversely, the pristine HY catalyst was suspended only in the glycerol phase because of its abundant silanol groups; the confinement of HY to the glycerol was another indication of its hydrophilicity. Previous work has shown that hydrophobic solid particles (contact angle > 90°) stabilize the formation of water-in-oil emulsions [41,61]. We hypothesized that the high degree of hydrophobicity of OTS-HY catalysts would stabilize an emulsion between glycerol and acetone.

Thus, we investigated emulsion formation by placing the OTS-HY catalyst in the aforesaid same two liquid systems: (1) water-dodecane; and (2) glycerol-acetone. First, we used a non-ionic surfactant, Tween 60, as a control. For the water-dodecane system, we added 1 wt.% Tween 60 and vortexed for one min. The microscopic images, taken after leaving this system for 30 min, showed water droplets dispersed in the dodecane, indicating the formation of a stable emulsion layer (Fig. S5C). Similarly, OTS-HY also stabilized the formation of the emulsion layer in the water-dodecane system (Fig. S5A). These results suggested that the OTS-HY catalyst assisted in the formation of Pickering emulsion in the water-dodecane system [62–65]. In contrast, in the glycerol-acetone system, after adding either Tween 60 or OTS-HY and vortexing for one min, we initially observed the formation of emulsion layer. However, this emulsion layer broke and separated back into two phases after stopping agitation (Fig. S5B & D) (*See Video2, Supplementary Information*).

The formation of Pickering emulsion has many benefits in two-phase reaction systems in which mass transfer limitation (limited contact between reactants) inhibits reactivity. For example, the use of solid particles, such as OTS-HY, to stabilize the emulsion enables easy breaking of the emulsion and recovery of the two phases. Moreover, this approach improves the contact between the two immiscible reactants without adding surfactants. Although adding surfactants in two-phase reactions can improve the contact between immiscible liquid reactants, adding surfactants complicates the downstream product purification and adds to the carbon footprint of the process [66].

3.3. Catalytic activity of OTS-HY catalysts in glycerol acetalization

Next, we demonstrated the benefit of the emulsion formation by OTS-HY in glycerol acetalization under reaction conditions. At 30 °C upon agitation after 10 s, OTS-HY began dispersing in the glycerol (bottom phase) and forming an emulsion (*See Video1, Supplementary Information*). Conversely, the HY only stayed in the glycerol phase regardless of the reaction time (Fig. S6). An increase in reaction temperature to 50 °C improved the glycerol solubility in acetone and enabled the emulsion formation by OTS-HY after 10 s (Fig. S7). Moreover, a 50 °C reaction temperature caused a larger HY suspension area compared with the area at 30 °C, indicating that increasing reaction temperature increased glycerol solubility in acetone and enabled more contact area between catalyst active sites and the two reactants. After 1 min, HY was well-dispersed in both phases (Fig. S7C). A further increase in reaction temperature to 70 °C enabled the higher glycerol solubility in acetone caused HY to be well-dispersed in both phases after 10 s (Fig. S8). These results suggested that the OTS-HY catalysts *itself* assisted in emulsion formation, thus eliminating the need for higher reaction temperatures.

The emulsion formation resulted in better contact between reactants with active sites of catalysts, leading to an improvement in the catalyst activity (Fig. 5A & B). We applied OTS-HY catalyst to glycerol acetalization at 30 °C and 12 wt.% glycerol for 600 min (10 h). We arbitrarily chose the 12 wt.% glycerol in acetone to provide excess acetone. We performed similar experiments with HY catalyst as control. Solketal was the main reaction product with a trace amount of 6-MR (Table 2). Glycerol conversion increased with increasing reaction time and leveled

Table 2
The glycerol conversion and products selectivity of investigated catalysts as a function of temperature and time. Reaction condition: 5 wt.% catalyst loading, acetone/glycerol molar ratio of 12/1.

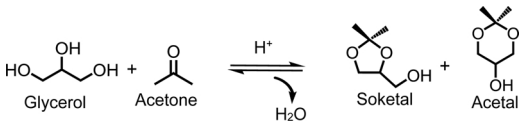

Catalyst	Temp. (°C)	Time (min)	Glycerol conv. (%)	Selectivity (%)	
				Solketal	Acetal
HY	30	10	7	83	17
		20	10	87	13
		60	28	88	12
		480	85	92	8
		600	89	98	2
HY	50	10	60	93	7
		20	65	94	6
		60	88	98	2
		480	88	98	2
		600	88	98	2
OTS-HY	30	10	73	88	12
		20	78	92	8
		60	89	95	5
		120	89	96	4
		480	89	98	2

Note: Temp. = Temperature; Glycerol conv. = Glycerol conversion.

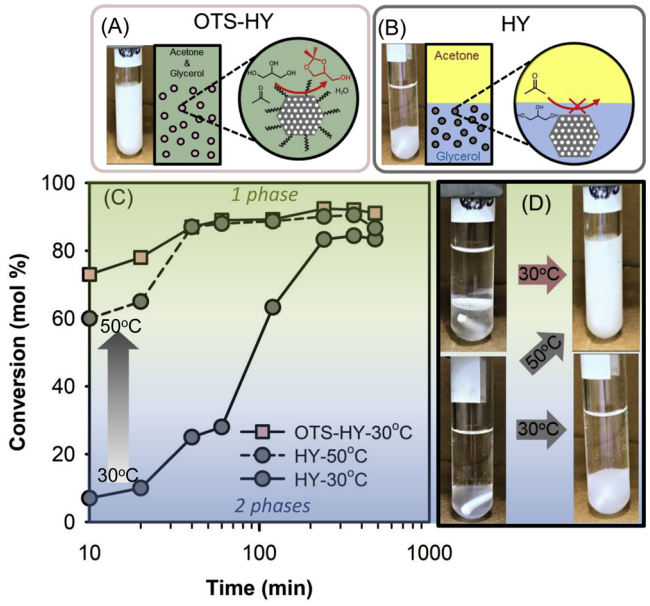

Fig. 5. Suspension behaviour of OTS-HY and HY catalysts in the glycerol-acetone system (A & B). Glycerol conversion by OTS-HY and HY catalysts over time (C). Changes in suspension behaviour of HY at 30 and 50 °C (D).

off at 89% after 60 min for OTS-HY catalyst at 30 °C (Fig. 5C). This plateau suggested that the reaction equilibrium was approached after 60 min. Our equilibrium conversion of 89% over the OTS-HY catalyst at 30 °C was consistent with the previously reported value [67].

In the case of HY catalyst at 30 °C, the reaction conversion reached 89% after 10 h. An increase in reaction temperature to 50 °C yielded the glycerol conversion of 88% after 60 min. These results suggested that using OTS-HY catalysts reached equilibrium faster than HY catalysts at 30 °C. Moreover, glycerol acetalization is an exothermic reaction. We observed the equilibrium conversion decreased slightly with increasing temperature using HY catalysts at 720 min (12 h) (Fig. 5C). This slight decrease in equilibrium conversion (< 2%) at elevated temperature was consistent with previous studies in both flow reactor with ethanol as a solvent and solvent-free batch reactor [67–69]. An increase in reaction temperature from 30 to 50 °C simply improved the reaction rates. We observed the evolution of the phases during the course of the reaction. At 12 wt.% glycerol in acetone, the system was a two-phase system. At 30 °C, the two-phase glycerol-acetone system became one phase after 60 min using OTS-HY catalysts, consistent with the 89% glycerol conversion. In the case of HY catalyst at 30 °C, the reaction system remained two phases even after 60 min, consistent with the 28% glycerol conversion. Consistent with the glycerol conversion results, these findings suggested the faster reaction rate was achieved by OTS-HY catalysts.

An increase in reaction temperature from 30 to 50 °C raised the catalytic activity of HY to nearly that of OTS-HY catalyst at 30 °C (Fig. 5D). One reason for this increased activity of HY was that an increase in temperature increased the glycerol solubility in acetone, enhancing the contact between HY's active sites and both reactants. Yu et al. reported a similar behaviour for SDS surfactants adsorbed on the surface of multi-wall carbon nanotubes (MWCNTs) that enhanced suspension of MWCNTs in aqueous solution [70].

3.4. Phase transition in glycerol acetalization due to the formation of solketal

Another important consideration was whether the formation of the product, solketal, affected the transition from two immiscible phases to one single phase during the reaction. We performed a series of experiments to demonstrate the behavior of the reaction mixture at varying reactants (glycerol and acetone) and products (solketal and water) concentration (i.e., simulated glycerol conversion between 0–100%) (Fig. 6). On the existence of the two immiscible phases, a slow mass transfer of acetone to glycerol phase was indicated at the beginning of the reaction because of a small supply of acetone. Upon the emulsion formation, the accumulation of the acetone in the glycerol phase promoted an increase in the overall rate. During the reaction, solketal is formed and accumulated. When the solketal yield exceeded 25%, it behaved as a solubilizing agent to make a homogenous mixture between glycerol and acetone, followed by a rapid conversion of glycerol because the interfacial mass transfer was eliminated.

We further explored how this phase transition affected the interfacial mass transfer limitations in glycerol acetalization over HY catalysts at 30 °C. When we performed the reaction under two-phase system

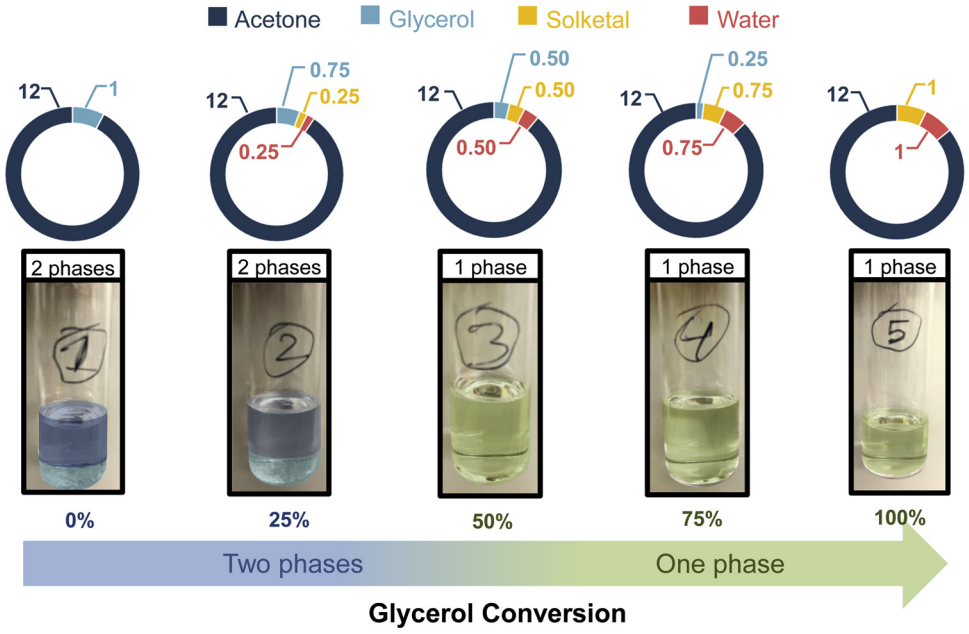

Fig. 6. Phase transition of the glycerol-acetone mixture during the course of reaction.

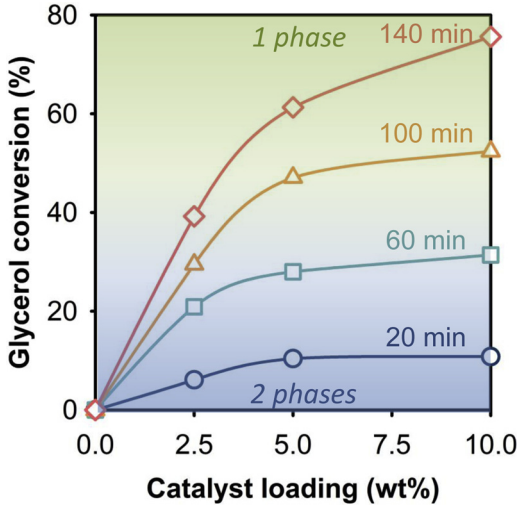

Fig. 7. Effect of catalyst loading on the glycerol conversion between 20–140 min.

(i.e., conversion < 25%, see Fig. 7), the glycerol conversion increased with increasing the catalyst loading only up to 5 wt.%. The higher amount of catalyst loading did not increase the glycerol conversion, suggesting that the reaction was controlled by the mass transfer of the reactant from one phase to the other (i.e., the mass transfer of acetone to the glycerol phase). However, when the reaction proceeded and conversion is > 50%, the glycerol conversion continuously increased with increasing catalyst loading because the interfacial mass transfer limitation was minimized (i.e., the initial two-phase system became homogenous (a single-phase) and the reaction became kinetically-controlled. These findings supported the existence of interfacial mass transfer limitations. Moreover, these results are consistent with the phase change behavior over the course of the reaction time (Fig. 6), affecting the apparent reaction rates.

Previous investigators have proposed the use of solvent (methanol, ethanol, and/or dichloromethane) to improve miscibility of glycerol and acetone, overcoming the mass transfer limitation of the glycerol acetalization [71,72]. Glycerol conversion reached 73% at 40 °C because the reaction rate was increased by both reactants being in the same phase [72]. However, the use of solvents to enhance the miscibility of glycerol and acetone complicates downstream processing because of additional unit operations for product separation/purification. Our hydrophobically modified zeolite catalysts had higher catalytic activity for glycerol acetalization than that of HY catalysts at low temperature because OTS-HY catalysts possessed two key advantages. First, the grafted hydrophobic layers of OTS-HY catalysts form emulsion between two immiscible reactants, minimizing the mass transfer limitation by improving contacts between the two immiscible reactants without added solvents. Second, the OTS-HY catalysts still had the comparable acid site density to that of HY, enabling the glycerol acetalization at the interface of two immiscible reactants. The high catalytic activity of OTS-HY at low temperatures makes it a promising candidate for glycerol acetalization and other acid-catalyzed two-phase reactions. The alkyl chain length of the organosilane surfactant affects the degree of hydrophobicity of the catalysts. We are currently correlating the degree of hydrophobicity of the modified catalyst with its catalytic activity in glycerol acetalization.

4. Conclusion

Acetalization of glycerol with acetone is an acid-catalyzed reaction. The poor miscibility between glycerol and acetone results in an initial two-phase mixture and presents a considerable interfacial mass transfer limitation between liquid phases and catalyst's active sites. Initially, the poor miscibility of acetone in glycerol phase caused a slow supply of acetone for the formation of solketal. When the solketal content exceeded 25%, it acted as a solubilizing agent and the reaction mixture became homogeneous, followed by a rapid production of solketal. We proposed to overcome this initial interfacial mass transfer limitation by grafting the n-octadecyltrichlorosilane (OTS) onto an HY catalyst. The modified HY catalyst was hydrophobic and assisted the emulsion formation during agitation. The emulsion formation improved the contact between the ordinarily immiscible reactants and active sites of the OTS-HY catalyst, yielding 89% glycerol conversion, compared with 28% for unmodified HY, at 30 °C. In addition, we revealed that the formation of reaction product, solketal, beyond 25% acted as a solvent to solubilize glycerol and acetone into a single phase. Hydrophobic zeolites of this type are promising for other acid-catalyzed reactions to upgrade by-product glycerol from biodiesel industry, such as esterification, dehydration to acrolein, and etherification with alcohols to produce fuel additives.

CRediT authorship contribution statement

Mohammad Shahinur Rahaman: Investigation, Formal analysis. **Thanh Khoa Phung:** Investigation, Formal analysis, Writing - original draft. **Md. Anwar Hossain:** Investigation, Formal analysis. **Emtias Chowdhury:** Investigation. **Sarttrawut Tulaphol:** Conceptualization, Methodology, Validation, Visualization. **Shashi B. Lalvani:** Conceptualization, Supervision. **Martin O'Toole:** Supervision. **Gerald A. Willing:** Supervision. **Jacek B. Jasinski:** Methodology, Investigation, Visualization. **Mark Crocker:** Conceptualization, Writing - review & editing, Supervision. **Noppadon Sathitsuksanoh:** Conceptualization, Methodology, Writing - review & editing, Supervision, Project administration.

Acknowledgment

A part of this material is based upon work supported by the National Science Foundation under Cooperative Agreement No. 1355438. This work was performed in part at the Conn Center for Renewable Energy Research at the University of Louisville, which belongs to the National Science Foundation NNCI KY Manufacturing and Nano Integration Node, supported by ECCS-1542174. The authors would like to thank Dr. Howard Fried for his valuable comments and suggestions on the manuscript.

Appendix A. Supplementary data

Supplementary material related to this article can be found, in the online version, at doi:https://doi.org/10.1016/j.apcata.2019.117369.

References

[1] M.M. Rojas-Downing, A.P. Nejadhashemi, T. Harrigan, S.A. Woznicki, Climate change and livestock: Impacts, adaptation, and mitigation, Clim. Risk Manage. 16 (2017) 145–163.
[2] U.S. Environmental Protection Agency, Inventory of U.S. Greenhouse Gas Emissions and Sinks: 1990-2017, Executive Summary, (2019) . (access Nov 19, 2019) https://www.epa.gov/ghgemissions/inventory-us-greenhouse-gas-emissions-and-sinks-1990-2017.
[3] A. Paquette, J. Vayreda, L. Coll, C. Messier, J. Retana, Climate change could negate positive tree diversity effects on forest productivity: a study across five climate types in Spain and Canada, Ecosystems 21 (2018) 960–970.
[4] C. Nolan, J.T. Overpeck, J.R. Allen, P. Anderson, J. Betancourt, H. Binney, S. Brewer, M. Bush, B. Chase, R. Cheddadi, Past and future global transformation of terrestrial ecosystems under climate change, Science 361 (2018) 920–923.
[5] O. Edenhofer, Climate Change 2014: Mitigation of Climate Change, Cambridge University Press, 2015.
[6] T. Boden, R. Andres, G. Marland, Global, Regional, and National Fossil-fuel CO_2 Emissions (1751-2014)(v. 2017), Oak Ridge, TN: Carbon Dioxide Information Analysis Center (CDIAC), Oak Ridge National Laboratory (ORNL), 2017.
[7] K. Anderson, G. Peters, The trouble with negative emissions, Science 354 (2016) 182–183.

[8] R.W. Howarth, Ideas and perspectives: is shale gas a major driver of recent increase in global atmospheric methane? Biogeosci. 16 (2019) 3033–3046.
[9] U.S.E.I. Administration, Monthly Biodiesel Production Survey, (2018).
[10] F. Yang, M.A. Hanna, R.C. Sun, Value-added uses for crude glycerol–a byproduct of biodiesel production, Biotechnol, Biotechnol. Biofuels 5 (2012) 13.
[11] M. Ayoobi, I. Schoegl, Non-catalytic conversion of glycerol to syngas at intermediate temperatures: Numerical methods with detailed chemistry, Fuel 195 (2017) 190–200.
[12] M.R.K. Estahbanati, M. Feilizadeh, M.C. Iliuta, Photocatalytic valorization of glycerol to hydrogen: Optimization of operating parameters by artificial neural network, Appl. Catal. B 209 (2017) 483–492.
[13] S. García-Fernández, I. Gandarias, J. Requies, F. Soulimani, P. Arias, B. Weckhuysen, The role of tungsten oxide in the selective hydrogenolysis of glycerol to 1, 3-propanediol over $Pt/WO_x/Al_2O_3$, Appl. Catal. B 204 (2017) 260–272.
[14] M. Massa, A. Andersson, E. Finocchio, G. Busca, Gas-phase dehydration of glycerol to acrolein over Al_2O_3-, SiO_2-, and TiO_2-supported Nb-and W-oxide catalysts, J. Catal. 307 (2013) 170–184.
[15] C.H. Zhou, J.N. Beltramini, Y.X. Fan, G.Q. Lu, Chemoselective catalytic conversion of glycerol as a biorenewable source to valuable commodity chemicals, Chem. Soc. Rev. 37 (2008) 527–549.
[16] D.C. de Carvalho, A.C. Oliveira, O.P. Ferreira, J.M. Filho, S. Tehuacanero-Cuapa, A.C. Oliveira, Tehuacanero-Cuapa, A.C. Oliveira, Titanate nanotubes as acid catalysts for acetalization of glycerol with acetone: Influence of the synthesis time and the role of structure on the catalytic performance, Chem. Eng. J. 313 (2017) 1454–1467.
[17] G.P. da Silva, M. Mack, J. Contiero, A promising and abundant carbon source for industrial microbiology, Biotechnol. Adv. 27 (2009) 30–39.
[18] V.K. Garlapati, U. Shankar, A. Budhiraja, Bioconversion technologies of crude glycerol to value added industrial products, Biotechnol. Rep. Amst. (Amst) 9 (2016) 9–14.
[19] M. da Silva, F. de Ávila Rodrigues, A. Júlio, SnF_2-catalyzed glycerol ketalization: A friendly environmentally process to synthesize solketal at room temperature over on solid and reusable Lewis acid, Chem. Eng. J. 307 (2017) 828–835.
[20] T.N. Pham, T. Sooknoi, S.P. Crossley, D.E. Resasco, Ketonization of carboxylic acids: mechanisms, catalysts, and implications for biomass conversion, ACS Catal. 3 (2013) 2456–2473.
[21] M.R. Nanda, Y. Zhang, Z. Yuan, W. Qin, H.S. Ghaziaskar, C. Xu, Catalytic conversion of glycerol for sustainable production of solketal as a fuel additive: A review, Renew. Sustain. Energy Rev. 56 (2016) 1022–1031.
[22] S. Gadamsetti, N.P. Rajan, G.S. Rao, K.V.R. Chary, Acetalization of glycerol with acetone to bio fuel additives over supported molybdenum phosphate catalysts, J. Mol. Cat. A Chem. 410 (2015) 49–57.
[23] M. Gonçalves, R. Rodrigues, T.S. Galhardo, W.A. Carvalho, Highly selective acetalization of glycerol with acetone to solketal over acidic carbon-based catalysts from biodiesel waste, Fuel 181 (2016) 46–54.
[24] C.J.A. Mota, C.X.A. da Silva, N. Rosenbach, J. Costa, F. da Silva, Glycerin Derivatives as Fuel Additives: The Addition of Glycerol/Acetone Ketal (Solketal) in Gasolines, Energy Fuel. 24 (2010) 2733–2736.
[25] P.H.R. Silva, V.L.C. Gonçalves, C.J.A. Mota, Glycerol acetals as anti-freezing additives for biodiesel, Bioresour. Technol. 101 (2010) 6225–6229.
[26] L. Fertier, M. Ibert, C. Buffe, R. Saint-Loup, C. Joly-Duhamel, J.J. Robin, O. Giani, New biosourced UV curable coatings based on isosorbide, Prog. Org. Coat. 99 (2016) 393–399.
[27] B.A.J. Noordover, A. Heise, P. Malanowksi, D. Senatore, M. Mak, L. Molhoek, R. Duchateau, C.E. Koning, R.A.T.M. van Benthem, Biobased step-growth polymers in powder coating applications, Prog. Org. Coat. 65 (2009) 187–196.
[28] M. Durand, V. Molinier, T. Féron, J.-M. Aubry, Isosorbide mono- and di-alkyl ethers, a new class of sustainable coalescents for water-borne paints, Prog. Org. Coat. 69 (2010) 344–351.
[29] J.I. Garcia, H. Garcia-Marin, E. Pires, Glycerol based solvents: synthesis, properties and applications, Green Chem. 16 (2014) 1007–1033.
[30] C. Chen, J.-T. Hu, Y.-J. Tu, J.-C. Wu, J. Liang, L.-L. Gao, Z.-G. Wang, B.-F. Yang, D.-L. Dong, Effects of isosorbide mononitrate on the restoration of injured artery in mice in vivo, Eur. J. Pharm. 640 (2010) 150–156.
[31] Z.Q. Li, X. He, X. Gao, Y.Y. Xu, Y.-F. Wang, H. Gu, R.-F. Ji, S.-J. Sun, Study on dissolution and absorption of four dosage forms of isosorbide mononitrate: Level A in vitro–in vivo correlation, Eur. J. Pharm. Biopharm. 79 (2011) 364–371.
[32] S.-A. Park, J. Choi, S. Ju, J. Jegal, K.M. Lee, S.Y. Hwang, D.X. Oh, J. Park, Copolycarbonates of bio-based rigid isosorbide and flexible 1,4-cyclohexanedimethanol: Merits over bisphenol-A based polycarbonates, Polymer 116 (2017) 153–159.
[33] C. da Silva, V. Gonçalves, C. Mota, Water-tolerant zeolite catalyst for the acetalisation of glycerol, Green Chem. 11 (2009) 38–41.
[34] C. Ferreira, A. Araujo, V. Calvino-Casilda, M. Cutrufello, E. Rombi, A. Fonseca, M. Bañares, I.C. Neves, Y zeolite-supported niobium pentoxide catalysts for the glycerol acetalization reaction, Microporous Mesoporous Mater. 271 (2018) 243–251.
[35] C.-N. Fan, C.-H. Xu, C.-Q. Liu, Z.-Y. Huang, J.-Y. Liu, Z.-X. Ye, Catalytic acetalization of biomass glycerol with acetone over TiO2–SiO2 mixed oxides, Reac. Kinet. Mech. Cat. 107 (2012) 189–202.
[36] A. Behr, D. Obst, B. Turkowski, Isomerizing hydroformylation of trans-4-octene to n-nonanal in multiphase systems: acceleration effect of propylene carbonate, J. Mol. Catal. A Chem. 226 (2005) 215–219.
[37] C. Sievers, Y. Noda, L. Qi, E. Albuquerque, R. Rioux, S. Scott, Phenomena affecting catalytic reactions at solid–liquid interfaces, ACS Catal. 6 (2016) 8286–8307.
[38] N. Weeranoppanant, Enabling tools for continuous-flow biphasic liquid–liquid reaction, React. Chem. Eng. 4 (2019) 235–243.
[39] M. Moreira, R. Faria, A. Ribeiro, A. Rodrigues, Solketal Production from Glycerol Ketalization with Acetone: Catalyst Selection and Thermodynamic and Kinetic Reaction Study, Ind. Eng. Chem. Res. 58 (2019) 17746–17759.
[40] H.C. Genuino, S. Thiyagarajan, J.C. van der Waal, E. de Jong, J. van Haveren, D.S. van Es, B.M. Weckhuysen, P. Bruijnincx, Selectivity Control in the Tandem Aromatization of Bio-Based Furanics Catalyzed by Solid Acids and Palladium, ChemSusChem 10 (2017) 277–286.
[41] P.A. Zapata, Y. Huang, M.A. Gonzalez-Borja, D.E. Resasco, Silylated hydrophobic zeolites with enhanced tolerance to hot liquid water, J. Catal. 308 (2013) 82–97.
[42] H. Wang, H. Ruan, M. Feng, Y. Qin, H. Job, L. Luo, C. Wang, M. Engelhard, E. Kuhn, X. Chen, M. Tucker, B. Yang, One-Pot Process for Hydrodeoxygenation of Lignin to Alkanes Using Ru-Based Bimetallic and Bifunctional Catalysts Supported on Zeolite Y, ChemSusChem 10 (2017) 1846–1856.
[43] P. Prinsen, R. Luque, C. González-Arellano, Zeolite catalyzed palmitic acid esterification, Microporous Mesoporous Mater. 262 (2018) 133–139.
[44] E. Pires, J. Magalhães, U. Schuchardt, Effects of oxidant and solvent on the liquid-phase cyclohexane oxidation catalyzed by Ce-exchanged zeolite Y, Appl. Catal. A Gen. 203 (2000) 231–237.
[45] E. Astorino, J.B. Peri, R.J. Willey, G. Busca, Spectroscopic Characterization of Silicalite-1 and Titanium Silicalite-1, J. Catal. 157 (1995) 482–500.
[46] T.K. Phung, M.M. Carnasciali, E. Finocchio, G. Busca, Catalytic conversion of ethyl acetate over faujasite zeolites, Appl. Catal. A Gen. 470 (2014) 72–80.
[47] M. Junaidi, C. Khoo, C. Leo, A. Ahmad, The effects of solvents on the modification of SAPO-34 zeolite using 3-aminopropyl trimethoxy silane for the preparation of asymmetric polysulfone mixed matrix membrane in the application of CO_2 separation, Microporous Mesoporous Mater. 192 (2014) 52–59.
[48] D. Flinn, D. Guzonas, R.-H. Yoon, Characterization of silica surfaces hydrophobized by octadecyltrichlorosilane, Colloids Surf. A Physicochem. Eng. Asp. 87 (1994) 163–176.
[49] A. Kumar, J. Richter, J. Tywoniak, P. Hajek, S. Adamopoulos, U. Šegedin, M. Petrič, Surface modification of Norway spruce wood by octadecyltrichlorosilane (OTS) nanosol by dipping and water vapour diffusion properties of the OTS-modified wood, Holzforschung 72 (2017) 45–56.
[50] K. Yamagishi, S. Namba, T. Yashima, Defect sites in highly siliceous HZSM-5 zeolites: a study performed by alumination and IR spectroscopy, J. Phys. Chem. 95 (1991) 872–877.
[51] T. Montanari, E. Finocchio, G. Busca, Infrared spectroscopy of heterogeneous catalysts: acidity and accessibility of acid sites of faujasite-type solid acids, J. Phys. Chem. C 115 (2010) 937–943.
[52] T. Korányi, F. Moreau, V. Rozanov, E. Rozanova, Identification of SH groups in zeolite-supported HDS catalysts by FTIR spectroscopy, J. Mol. Struct. 410-411 (1997) 103–110.
[53] M. Makarova, A. Ojo, K. Karim, M. Hunger, J. Dwyer, FTIR study of weak hydrogen bonding of Broensted hydroxyls in zeolites and aluminophosphates, J. Phys. Chem. 98 (1994) 3619–3623.
[54] I. Tsuchiya, Infrared spectroscopic study of hydroxyl groups on silica surfaces, J. Phys. Chem. 86 (1982) 4107–4112.
[55] I.-S. Chuang, G.E. Maciel, Probing hydrogen bonding and the local environment of silanols on silica surfaces via nuclear spin cross polarization dynamics, JACS 118 (1996) 401–406.
[56] S. Mirji, S. Halligudi, D.P. Sawant, N.E. Jacob, K. Patil, A. Gaikwad, S. Pradhan, Adsorption of octadecyltrichlorosilane on mesoporous SBA-15, Appl. Surf. Sci. 252 (2006) 4097–4103.
[57] J. Parise, D. Corbin, L. Abrams, D. Cox, Structure of dealuminated Linde Y-zeolite; Si139. 7Al52. 3O384 and Si173. 1Al18. 9O384: presence of non-framework Al species, Acta Crystallogr, Sect. C: Cryst. Struct. Commun 40 (1984) 1493–1497.
[58] V. Felice, A.C. Tavares, Faujasite zeolites as solid electrolyte for low temperature fuel cells, Solid State Ion. 194 (2011) 53–61.
[59] P.A. Zapata, J. Faria, M.P. Ruiz, R.E. Jentoft, D.E. Resasco, Hydrophobic zeolites for biofuel upgrading reactions at the liquid–liquid interface in water/oil emulsions, JACS 134 (2012) 8570–8578.
[60] N.-Y. Topsøe, K. Pedersen, E.G. Derouane, Infrared and temperature-programmed desorption study of the acidic properties of ZSM-5-type zeolites, J. Catal. 70 (1981) 41–52.
[61] B. Binks, S. Lumsdon, Catastrophic phase inversion of water-in-oil emulsions stabilized by hydrophobic silica, Langmuir 16 (2000) 2539–2547.
[62] B. Binks, J. Rodrigues, W. Frith, Synergistic interaction in emulsions stabilized by a mixture of silica nanoparticles and cationic surfactant, Langmuir 23 (2007) 3626–3636.
[63] S. Arditty, C. Whitby, B. Binks, V. Schmitt, F. Leal-Calderon, Some general features of limited coalescence in solid-stabilized emulsions, Eur. Phys. J. E 11 (2003) 273–281.
[64] B. Binks, J. Clint, from surface energy components: relevance to Pickering emulsions, Langmuir 18 (2002) 1270–1273.
[65] S. Pickering, Chem, J. Chem. Soc., Trans. 91 (1907) 2001–2021.
[66] M. Pera-Titus, L. Leclercq, J.M. Clacens, F. De Campo, V. Nardello-Rataj, Pickering interfacial catalysis for biphasic systems: from emulsion design to green reactions, Angew. Chem. Int. Ed. 54 (2015) 2006–2021.
[67] A. Cornejo, M. Campoy, I. Barrio, B. Navarrete, J. Lázaro, Solketal production in a solvent-free continuous flow process: scaling from laboratory to bench size, React. Chem. Eng. (2019).
[68] I. Agirre, I. Garcia, J. Requies, V. Barrio, M. Güemez, J. Cambra, P. Arias, Glycerol acetals, kinetic study of the reaction between glycerol and formaldehyde, Biomass Bioenergy 35 (2011) 3636–3642.
[69] I. Agirre, M. Güemez, A. Ugarte, J. Requies, V. Barrio, J. Cambra, P. Arias, Glycerol

acetals as diesel additives: Kinetic study of the reaction between glycerol and acetaldehyde, Fuel Process. Technol 116 (2013) 182–188.
[70] J. Yu, N. Grossiord, C.E. Koning, J. Loos, Controlling the dispersion of multi-wall carbon nanotubes in aqueous surfactant solution, Carbon 45 (2007) 618–623.
[71] M. Nanda, Z. Yuan, W. Qin, H. Ghaziaskar, M.-A. Poirier, C. Xu, Thermodynamic and kinetic studies of a catalytic process to convert glycerol into solketal as an oxygenated fuel additive, Fuel 117 (2014) 470–477.
[72] J. Deutsch, A. Martin, H. Lieske, Investigations on heterogeneously catalysed condensations of glycerol to cyclic acetals, J. Catal. 245 (2007) 428–435.